

# Deep Event Visual Odometry

Simon Klenk<sup>1,2\*</sup> Marvin Motzet<sup>1,2\*</sup> Lukas Koestler<sup>1,2</sup> Daniel Cremers<sup>1,2</sup>

<sup>1</sup>Technical University of Munich <sup>2</sup>Munich Center for Machine Learning

{simon.klenk, marvin.motzet, lukas.koestler, cremers}@tum.de

## Abstract

Event cameras offer the exciting possibility of tracking the camera’s pose during high-speed motion and in adverse lighting conditions. Despite this promise, existing event-based monocular visual odometry (VO) approaches demonstrate limited performance on recent benchmarks. To address this limitation, some methods resort to additional sensors such as IMUs, stereo event cameras, or frame-based cameras. Nonetheless, these additional sensors limit the application of event cameras in real-world devices since they increase cost and complicate system requirements. Moreover, relying on a frame-based camera makes the system susceptible to motion blur and HDR. To remove the dependency on additional sensors and to push the limits of using only a single event camera, we present Deep Event VO (DEVO), the first monocular event-only system with strong performance on a large number of real-world benchmarks. DEVO sparsely tracks selected event patches over time. A key component of DEVO is a novel deep patch selection mechanism tailored to event data. We significantly decrease the pose tracking error on seven real-world benchmarks by up to 97% compared to event-only methods and often surpass or are close to stereo or inertial methods.

## 1. Introduction

Event cameras are visual sensors with high temporal resolution, high dynamic range, low latency, and low energy consumption. Hence, event cameras are ideally suited for unlocking several spatial computing applications in robotics or AR/VR, which are currently inaccessible for traditional frame-based cameras. A key component for spatial computing is visual odometry (VO), which estimates 6-dof camera poses from a visual data stream [4]. The estimated poses are required by different downstream tasks, *e.g.*, motion planning and control in robotics, or photorealistic rendering of virtual objects in VR applications. A primary challenge of existing VO systems is their limited robustness to motion blur and high dynamic range (HDR). These problem-

atic scenarios can be substantially alleviated by utilizing an event camera instead of a conventional frame-based camera. Event cameras report per-pixel, asynchronous brightness changes above or below a camera-internal threshold with microsecond resolution, resulting in a large dynamic range. Therefore, event cameras are less susceptible to motion blur and HDR [15, 56].

Existing event-based VO methods [7, 21, 24, 42, 56] have shown to increase the robustness of camera pose estimation in adverse conditions. However, most of these methods rely on additional sensors for good performance, such as a frame-based camera [24], an IMU [21], an IMU and a frame-based camera [56], or an IMU with a stereo event camera setup [7]. Relying on additional sensors has the disadvantage of increased cost and complicated system requirements, *e.g.*, requiring more space, higher energy density for powering all sensors, and more complicated calibration routines. Furthermore, systems relying on a frame-based camera are susceptible to motion blur and HDR.

In this work, we revisit the task of monocular event-only VO. We are motivated by the question: *What is the limit of general, real-world monocular event-only VO using no additional sensors?* Our work is inspired by the fact that events are close to optical flow in nature since events can be first-order approximated as dot product between optical flow and image brightness gradient [15]. Hence, we propose to base our VO system on optical flow estimation, inspired by frame-based systems such as BASALT [55], DROID-SLAM [52], DPVO [53], DF-VO [65], and Tartan-VO [60]. The main contributions of this paper are:

- We introduce a novel patch selection mechanism specifically tailored towards event data, which increases the accuracy and robustness of DEVO.
- DEVO is the first monocular, event-only method showing strong performance across *seven* real-world benchmarks.
- DEVO demonstrates that supervised learning on a large-scale dataset of simulated events enables strong generalization to real-world event VO benchmarks.
- We open-source our code (including training, evaluation, and event data generation) to foster further research in deep event-based VO.

\*Equal contribution. Code at: <https://github.com/tum-vision/DEVO>

## 2. Related Work

**Learning-based VO** Learning-based VO has shown to improve accuracy and robustness compared to classical, model-based VO [26]. Earlier approaches predict the pose end-to-end from images [54, 58, 67]. Drawing inspiration from the classical methods [12, 38], a beneficial approach has emerged to first predict correspondences and subsequently use these in a principled, geometry-based manner for pose prediction [52, 53, 60, 65]. This method utilizes the 3D geometry of the problem. Thus, it can avoid overfitting and increase robustness and generalization. Correspondence can either be explicitly modeled by feature points [9, 13, 22, 38] or implicitly defined by optical flow [52, 53, 55, 60, 65].

DROID-SLAM [52] proposes to incorporate a recurrent update operator [51] for iterative optical flow prediction and a differentiable bundle adjustment layer for pose estimation. DPVO [53] proposes a sparse version for the DROID-SLAM frontend, tracking sparse patches randomly extracted from RGB frames and estimating optical flow for these patches only. Sparsification improves memory usage and runtime. While DPVO shows strong performance, its evaluation is limited to two real-world datasets.

**Event-based VO using additional sensors** The majority of event-based VO systems rely on additional sensors. Weikersdorfer et al. [62] are the first to demonstrate event and depth VO on a small-scale custom dataset. Similarly, Zuo et al. [74] employ a depth and event sensor. Due to the scarcity of datasets containing both modalities, they only evaluate on MVSEC [70] and on their custom dataset.

Hidalgo et al. [24] combine frames and events using the generative event model and photometric bundle adjustment inspired by DSO [12]. Similarly, Kueng et al. [30] detect Harris corners [23] in DAVIS [1] frames and track those using events. A drawback of both methods is that specifically designed camera setups are required, either through dual pixel architecture [30] or through an optical beamsplitter with a large form factor with reduced incoming light [24]. Moreover, the problem of relying on frames is that the overall system is still susceptible to motion blur and HDR.

Inertial measurement units (IMUs) are either employed in the event-VO backend [20, 37, 73] or also for improved event feature tracking [31, 43, 64]. The problem of using an IMU is that the IMU bias parameter estimation is often difficult to achieve with sufficient accuracy, even with extensive parameter tuning [3, 57]. Further sensor combinations such as event and frames, events and IMU [21, 36, 56], or stereo event cameras and IMU [7] have been proposed. Using additional sensors tends to increase robustness since different modalities can complement each other.

**Monocular event-only VO** Estimating 6-dof poses from only event data is very challenging. Thus, some approaches rely on a known photometric 3D map [2, 14] or restrict

the motion type to rotation-only [27, 33, 34, 46], planar [14, 61], or forward-facing motion [72]. Kim et al. [28] propose an approach for full 6-dof pose tracking, utilizing three Kalman filters for estimating pose, intensity gradient, and depth, respectively. They assume a known contrast threshold and show qualitative results. The monocular event-only VO proposed by Rebecq et al. [42] is purely geometry-based, utilizing event-ray reprojection [41]. EVO can perform well on small-scale scenes, but it is very parameter-sensitive and requires bootstrapping, which is either achieved through a planar, fronto-parallel scene assumption or by using a frame-based camera.

Zhu et al. [71] and Ye et al. [63] employ a CNN to predict pose, flow, and depth using unsupervised learning on MVSEC [70]. Dense CNNs sacrifice event sparsity. Moreover, both methods fail to show generalization beyond the indoor flying scenes of MVSEC, which are also used for their training. In a similar fashion, Gelen et al. [18] propose a SLAM system that is trained and evaluated on scenes from the same simulated CARLA environment [10]. They utilize three CNNs for end-to-end pose, depth, and loop-closure estimation, respectively, and collapse the events data to 2D histograms, sacrificing their temporal resolution.

In contrast to the above deep event VO systems, our work is the only approach utilizing event sparsity. Moreover, we do not perform end-to-end pose prediction but utilize intermediate optical flow and differentiable bundle adjustment as in DPVO [53]. We are the only approach training on a very large dataset and thus are able to demonstrate generalization from simulation to several real-world benchmarks.

## 3. Deep Event Visual Odometry (DEVO)

Our approach extends DPVO [53] to the event modality. We propose a novel patch selection mechanism for sparse event data. Event data pose unique challenges, *e.g.*, a large sim-to-real gap [48]. We thus propose specific event augmentations during training and randomized event simulation.

### 3.1. Event Representation

Events are a stream of tuples  $(x_k, y_k, t_k, p_k)$ , indicating an increase ( $p_k = 1$ ) or decrease ( $p_k = -1$ ) of observed brightness at pixel  $\mathbf{u} = (x_k, y_k)$  with microsecond timestamp  $t_k$ . We process events to a sequence of volumetric voxel grids  $\{\mathbf{E}_t\}_{t=1}^N$  [71] for compatibility with standard neural networks, where  $\mathbf{E}_t \in \mathbb{R}^{H \times W \times 5}$ . Voxel grids preserve temporal information by bilinear interpolation of event counts in time. We discretize the time dimension into five bins and normalize each voxel grid to zero mean and unit variance. Each event voxel grid  $\mathbf{E}_t$  is assigned to a ground truth camera pose  $\mathbf{T}_t \in \mathbb{SE}(3)$  and a ground truth inverse depth map  $\mathbf{d}_t \in \mathbb{R}_+^{H \times W}$ . Note that in the following,  $\hat{\mathbf{T}}_t$  and  $\hat{\mathbf{d}}_t$  denote the predictions of  $\mathbf{T}_t$  and  $\mathbf{d}_t$ , respectively.

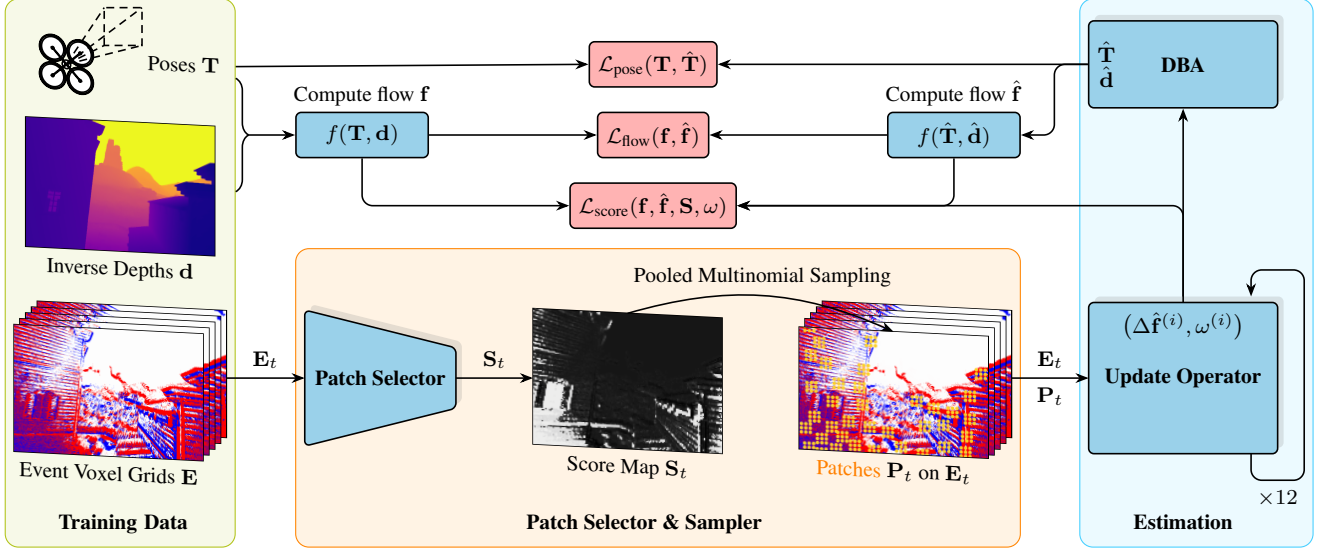


Figure 1. Overview of our proposed method. During training, DEVO takes event voxel grids  $\{\mathbf{E}_t\}_{t=1}^N$ , inverse depths  $\{\mathbf{d}_t\}_{t=1}^N$ , and camera poses  $\{\mathbf{T}_t\}_{t=1}^N$  of a sequence of size  $N$  as input. DEVO estimates poses  $\{\hat{\mathbf{T}}_t\}_{t=1}^N$  and depths  $\{\hat{\mathbf{d}}_t\}_{t=1}^N$  of the sequence. Our novel patch selection network predicts a score map  $\mathbf{S}_t$  to highlight optimal 2D coordinates  $\mathbf{P}_t$  for optical flow and pose estimation. A recurrent update operator iteratively refines the sparse patch-based optical flow  $\hat{\mathbf{f}}$  between event grids by predicting  $\Delta\hat{\mathbf{f}}$  and updates poses and depths through a differentiable bundle adjustment (DBA) layer, weighted by  $\omega$ , for each revision. Ground truth optical flow  $\mathbf{f}$  for supervision is computed using poses and depth maps. At inference, DEVO samples from a multinomial distribution based on the pooled score map  $\mathbf{S}_t$ .

**Photometric voxel augmentations** The ESIM [44] event simulator employs the event generation model [15]

$$\Delta L(\mathbf{u}_k, t_k) = L(\mathbf{u}_k, t_k) - L(\mathbf{u}_k, t_{k-1}) = p_k C, \quad (1)$$

where  $C$  is the camera-internal contrast threshold and  $L(\mathbf{u}, t) = \ln(\mathbf{I}_t[\mathbf{u}])$  is the logarithmic mapping of image brightness. ESIM tends to produce densely populated event voxels, especially in dark image regions, due to the logarithm in Eq. (1). Hence, the training dataset contains noticeably more densely populated event voxels than the real-world evaluation datasets. To reduce the sim-to-real gap, we augment the simulated voxels used for training with photometric augmentations, which reduce event density.

### 3.2. Deep Event Patch Selection

Frame-based methods such as DSO [12], LSD-SLAM [11], and DPVO [53] successfully utilize patches covering most of the image plane, which works well for dense data like RGB images. However, events frequently only sparsely cover the image plane (*cf.* Fig. 1), leaving large areas devoid of events. Tracking features in such non-discriminative areas often results in VO failures [17].

**Approach overview** We re-use the patch graph architecture and the iterative update operator from DPVO [53]. The dynamic patch graph  $(\mathcal{V}, \mathcal{E})$  connects event patches on  $\mathbf{E}_t$  with event voxel grids  $\mathbf{E}_{t'}$  such that  $t' \neq t$ . Patch trajectories, which form the correspondences for VO, are obtained by reprojecting a patch in all its connected event grids of the

patch graph. The update operator, a recurrent neural network, iteratively proposes revisions  $\Delta\hat{\mathbf{f}}$  to optical flow estimates  $\hat{\mathbf{f}}$ . Based on the most recent optical flow estimate, the differentiable bundle adjustment (DBA) layer [32, 50, 53] updates camera poses and patch depths of all patches within a sliding window of recent keyframes.

**Patch selection network** We propose a novel *patch selection network* to make sparse patch-based tracking accurate and robust for the event modality. The patch selection network predicts a *score map*  $\mathbf{S}_t \in [0, 1]^{H/4 \times W/4}$  of voxel grid  $\mathbf{E}_t$ , highlighting 2D coordinates which are optimal for optical flow and pose estimation. It consists of three convolutional layers of kernel size three, each followed by a ReLU. The voxel grids provide five input channels, which are progressively increased to [8, 16, 32] channels, respectively. The fourth convolutional layer outputs one channel and is followed by max-pooling with kernel size and stride of four. The network outputs the one-channel score map bounded to [0, 1] by using a sigmoid activation. The patch selection network is trained jointly with the overall system using a dedicated score loss  $\mathcal{L}_{\text{score}}$  (*cf.* Eq. (2)).

**Training the score map** We select  $P$  patch coordinates  $\mathbf{P}_t = \{\mathbf{p}_k^t\}_{k=1}^P$  per voxel grid  $\mathbf{E}_t$  based on the score values  $s_k = \mathbf{S}_t[\mathbf{p}_k^t]$ , where  $\mathbf{p}_k^t \in \mathbb{R}^{H/4 \times W/4}$ . We aim to predict high scores  $s_k$  at patch coordinates  $\mathbf{p}_k^t$  which are well-suited for tracking, *i.e.*, the optical flow residuals  $r_{k,j}$  of patch  $k$  onto voxel grid  $\mathbf{E}_j$  are small *and* the estimated confidence weights  $\omega_{k,j}$  of the DBA are large. To achieve this, we min-

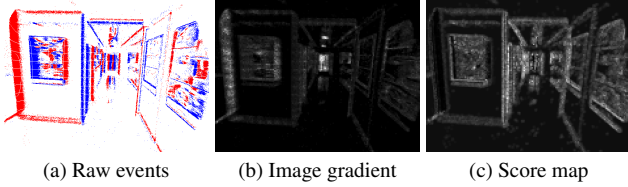


Figure 2. Comparison of gradient map (middle) and proposed score map (right) for event input (left). Selecting patches from our learned score map is more accurate and robust than from the gradient map (*cf.* Sec. 4.2).

imize score map values with large tracking error by multiplying the score  $s_k$  of patch  $k$  with the corresponding residuals  $r_{kj}$  and “inverted weight”  $(1 - \alpha \ln \omega_{kj})$ . Large score map values are enforced by subtracting the logarithm of the sampled score map values  $\mathbf{S_P} = \mathbf{S}[\mathbf{P}]$ :

$$\mathcal{L}_{\text{score}} = \frac{1}{|\mathcal{E}|} \sum_{(k,j) \in \mathcal{E}} s_k r_{kj} (1 - \alpha \ln \omega_{kj}) - \ln \mathbf{S_P}. \quad (2)$$

The term  $\alpha$  controls the influence of the DBA weights. Note that no ground truth labels for  $\mathbf{S}$  are needed for training.

During training, we first randomly evaluate  $3P$  patch coordinates and subsequently use the  $P$  patches with the highest value in the score map for tracking. We refer to this strategy as *3P-random*. Figure 2 shows the qualitative difference between our learned score map and a gradient map.

The total loss is given by  $\mathcal{L} = 0.05\mathcal{L}_{\text{score}} + 0.1\mathcal{L}_{\text{flow}} + 10\mathcal{L}_{\text{pose}}$ . While  $\mathcal{L}_{\text{flow}}$  and  $\mathcal{L}_{\text{pose}}$  are applied after each iteration of the update operator,  $\mathcal{L}_{\text{score}}$  is only applied after the last iteration. Ground truth optical flow of event patches is computed from camera poses and depth maps, see Fig. 1.

**Sampling from the score map** Sampled patches need to be broadly distributed over the entire image plane in order to achieve accurate VO [5, 35, 55]. Hence, we first subdivide the image plane into  $G$  disjoint grid cells before sampling. Within each grid cell, we sample  $\frac{P}{G}$  patches.

Moreover, we want to sample patches with high values in the score map since high values indicate relevant coordinates for tracking. This approach could be achieved by following the *3P-random* strategy of the training or by simply picking the  $P$  highest values in the score map (*top-P sampling*). However, both strategies are still sensitive to outliers, less accurate, and less robust on average (*cf.* Sec. 4.2) than our proposed *pooled multinomial sampling*.

Multinomial sampling models a multinomial distribution of score map values over 2D patch coordinates and subsequently samples  $P$  distinct 2D coordinates without replacement ( $\frac{P}{G}$  per grid cell). Multinomial sampling likely chooses high values in the score map, but it does not only choose the highest values. Hence, it is less sensitive to real-world outliers of the score map than *top-P sampling*.

Note that the score map’s resolution  $(H_{\text{sc}}, W_{\text{sc}})$  is one 1/4-th of the input resolution  $(H, W) = (4H_{\text{sc}}, 4W_{\text{sc}})$

as the feature map’s resolution in DPVO [53]. To further robustify the sampling procedure, we propose *pooled sampling*, which performs a  $4 \times 4$  average pooling with stride of four on the score map before multinomial sampling, resulting in a *pooled score map* of  $(H_{\text{pool}}, W_{\text{pool}}) = (H/16, W/16)$ . This smoothens score map values and increases the receptive field. For each sampled value in the pooled score map, we apply a second multinomial sampling on the corresponding  $4 \times 4$  window of the initial score map to get 2D coordinates of the resolution  $(H_{\text{sc}}, W_{\text{sc}})$ . Furthermore, pooled sampling has a performance advantage as sampling is performed at a small resolution  $(H_{\text{pool}}, W_{\text{pool}})$ . Since we sample distinct 2D coordinates without replacement in the pooled score map and patches in the score map are of size  $3 \times 3$ , we automatically avoid overlapping patches in the score map. The sampled patch coordinates are used to index the matching and context feature map as in DPVO [53].

**Implementation details** We simulate events on all sequences of the TartanAir dataset [59] using the ESIM [44] simulator. We randomize the contrast thresholds per sequence, sampling the negative and positive contrast thresholds independently from a uniform distribution in  $C \sim \mathcal{U}(0.16, 0.34)$ . We perform multi-GPU training for a total of 240,000 iterations on two A40s with a batch size of 1, sequence size  $N = 15$ , and  $P = 80$ , which takes 2.5 days. We apply a  $2 \times 2$  grid for sampling during evaluation.

## 4. Experiments

We evaluate DEVO on seven real-world event VO benchmarks while training in simulation only. We compare our method to multiple baselines from the literature, including methods using more sensors. We propose two additional baselines: (i) DPVO [53], which runs on the RGB frames of the respective dataset, (ii) DPVO<sup>†</sup> [45, 53], which is a re-trained DPVO model on the E2VID [45] reconstructions of all TartanAir sequences. The re-trained model runs on E2VID reconstructions of the respective target dataset. Different from DPVO [53], DEVO and the baselines (i) and (ii) are trained on *all* sequences of the TartanAir [59] dataset. To obtain high-quality reconstructions for DPVO<sup>†</sup> [45, 53], we only feed a subset of all events per grid into E2VID [45] for fast or high-resolution sequences.

### 4.1. Quantitative Evaluation

We intentionally refrain from parameter tuning to demonstrate generalization. We thus use the exact same parameter setting for all evaluation sequences, except the keyframe threshold, which we set to 5 on RPG [68], MVSEC [70] and UZH-FPV [8], to 25 on EDS [24] and to 15 on all other datasets. The keyframe threshold is specified in terms of the average optical flow, which is smaller for smaller resolution and slower motions.

Method	Modality	indoor_fwd						indoor_45_deg		
		3	5	6	7	9	10	2	4	9
ORB-SLAM3 [6]	Stereo VIO	0.55	1.19	–	<b>0.36</b>	0.77	1.02	2.18	1.53	<b>0.49</b>
VINS Fusion [40]	Stereo VIO	0.84	–	1.45	0.61	2.87	4.48	–	–	–
VINS Mono [39]	Mono VIO	0.65	1.07	<b>0.25</b>	<u>0.37</u>	0.51	0.92	<b>0.53</b>	1.72	1.25
DPVO [53]	Mono VO	–	–	–	–	–	–	–	–	–
USLAM [56]	Mono EVIO	–	–	–	–	–	–	–	9.79	4.74
PLEVIO [21]	Mono EVIO	<u>0.38</u>	0.90	<u>0.30</u>	0.55	<b>0.44</b>	1.06	<u>0.55</u>	1.30	<u>0.76</u>
EVO [42]	Mono EO	–	–	–	–	–	–	–	–	–
DPVO <sup>†</sup>	Mono EO <sup>†</sup>	0.52	<u>0.42</u>	0.55	–	<u>0.45</u>	<u>0.54</u>	–	<u>1.21</u>	–
<b>DEVO (ours)</b>	Mono EO	<b>0.37</b>	<b>0.40</b>	0.31	0.50	0.61	<b>0.52</b>	0.72	<b>0.45</b>	0.89

Table 1. UZH-FPV drone racing dataset [8] with MPE[%/m]. Baseline numbers are taken from [21].

On each dataset, we run five trials and report the median result. For monocular methods, the global scale is estimated once before alignment. We employ absolute trajectory error ATE[cm] ( $\downarrow$ ) [49], RMSE rotational error  $\mathbf{R}_{\text{rmse}}$ [deg] ( $\downarrow$ ) [66], and mean position error MPE[%/m] ( $\downarrow$ ) [7, 56], utilizing the EVO toolbox [19]. For stereo datasets, we employ the left camera stream. In the following tables, we highlight methods with access to additional sensors in gray and mark results with “–” to indicate a failure.

**UZH-FPV drone racing dataset** The UZH-FPV drone racing dataset [8] provides data from a DAVIS346 [1] mounted on a drone performing aggressive maneuvers at high speed. Table 1 shows that our method outperforms all related work on four of nine sequences. This is noteworthy because all other successful methods use an IMU, except our proposed event-only baseline DPVO<sup>†</sup>. DPVO<sup>†</sup> fails on three of nine sequences and performs worse than DEVO on eight of nine sequences. VINS Fusion [40] and ORB-SLAM3 [6] both employ stereo VIO, but usually they perform worse than DEVO. The event-based methods USLAM [56] and PLEVIO [21] have access to strictly more data than our method. However, both methods are still outperformed by DEVO on the majority of the sequences. We compare DEVO to other monocular methods, DPVO [53] and EVO [42], which both fail on all sequences.

**VECTor** The VECTor dataset [16] provides stereo events and frames captured by two Prophesee Gen3 and two high-quality, global shutter FLIR Grasshopper3 cameras. It covers a variety of aggressive motion and illumination changes for both small and large-scale scenes. As seen in Tab. 2, our proposed DEVO achieves outstanding results on most of the sequences under the fact that DEVO utilizes event data only while EVO [42] and ESVO [69] fail on 88% and 76% of the sequences, respectively. The baseline DPVO<sup>†</sup> fails on four sequences and struggles with the fast and large-scale sequences. Our method even beats ESVO [7] on 70% of the sequences, which utilize not only stereo events but also high-quality stereo frames and an IMU. DEVO performs better on average than DPVO on large-scale sequences but

is usually worse than DPVO on small-scale scenes. Please note that DPVO profits from the high-quality frames.

**HKU** The HKU dataset [7] is a collection of stereo event data and frames from two DAVIS346 [1], which contains scenes with extremely fast 6-dof motion and strong HDR. In Tab. 3, we compare to other event- and frame-based VO and VIO. Our method outperforms all previous work on five out of nine sequences. Other event-only VO methods, EVO and ESVO, fail on all sequences. DEVO fails with multinomial sampling on the very challenging sequence *agg\_walk*, where the baseline DPVO<sup>†</sup> and the two stereo VIO systems ORB-SLAM3 and VINS Fusion fail as well. However, with top- $P$  sampling, DEVO can track the poses of *agg\_walk* without failure. Moreover, we beat DPVO, especially on HDR scenes. DPVO fails on one sequence. The results on this dataset demonstrate the exciting potential of event-only methods for challenging capturing conditions.

**EDS** The EDS dataset [24] provides events from a handheld Prophesee Gen3.1. To the best of our knowledge, we provide the first results for pose estimation on EDS. In Tab. 4, we compare our method with ORB-SLAM3, DPVO<sup>†</sup>, and DPVO. While we beat DPVO<sup>†</sup> and perform similarly to DPVO on most sequences, we perform worse on *peanuts\_dark*, *peanuts\_light*, and *peanuts\_run*. Our method performs clearly better than DPVO on *rocket\_dark*, *ziggy\_hdr*, and *all\_chars* due to HDR and very fast motion.

**TUM-VIE** The TUM-VIE dataset [29] provides stereo events from two HD Prophesee Gen4. We show the results in Tab. 5. We beat all event-only methods (DPVO<sup>†</sup>, EVO, and ESVO) and USLAM by large margins on all presented sequences. We even outperform DH-PTAM [47] on four out of five sequences, even though DH-PTAM utilizes all four cameras of the setup (stereo EVO).

**RPG** The RPG dataset [68] provides events from a handheld stereo DAVIS240C [1]. Table 6 shows that we outperform the event-only methods DPVO<sup>†</sup>, EVO, and ESVO (stereo EO) by large margins on all sequences. Moreover, we outperform USLAM (mono EVIO) and EDSO [24] (mono EVO) on all sequences, and DPVO on three of four

Method Modality	ORB3 [6]	VINSFusion [40]	DPVO [53]	ESVIO [7]	PLEVIO [21]	ESVO [69]	EVO [42]	DPVO <sup>†</sup>	DEVO(ours)
	StereoVIO	StereoVIO	MonoVO	StereoEVIO	MonoEVIO	StereoEO	MonoEO	MonoEO <sup>†</sup>	MonoEO
	MPE/ATE	MPE/ATE	MPE/ATE	MPE/ATE	MPE/ATE	MPE/ATE	MPE/ATE	MPE/ATE	MPE/ATE
corner-slow	1.49 / <u>1.2</u>	1.61 / 1.3	<b>0.30 / 0.4</b>	1.49 / <u>1.2</u>	2.10 / 1.7	4.83 / 3.9	4.33 / 3.5	-/-	<u>0.59 / 1.2</u>
robot-norm	0.73 / 2.9	0.58 / 2.3	<b>0.15 / 0.7</b>	1.08 / 4.3	0.68 / 2.7	-/-	3.25 / 13.0	0.22 / 2.4	<u>0.17 / 1.0</u>
robot-fast	0.71 / 15.0	-/-	<b>0.07 / 1.7</b>	0.20 / 4.2	0.17 / <u>3.7</u>	-/-	-/-	0.73 / 18.9	<u>0.13 / 3.7</u>
desk-norm	0.46 / 3.9	0.47 / 4.0	<b>0.09 / 1.0</b>	0.61 / 5.2	3.66 / 31.0	-/-	-/-	0.18 / 2.6	<u>0.11 / 1.1</u>
desk-fast	0.31 / 9.9	0.32 / 10.0	<b>0.05 / 1.9</b>	<u>0.13 / 4.2</u>	0.14 / 4.3	-/-	-/-	0.77 / 30.2	0.15 / 6.1
sofa-norm	0.15 / 4.4	<u>0.13 / 3.8</u>	<b>0.06 / 2.1</b>	0.16 / 4.7	0.19 / 5.8	1.77 / 53.0	-/-	0.22 / 10.1	0.13 / 4.7
sofa-fast	0.21 / 6.4	0.57 / 17.0	<b>0.07 / 2.2</b>	0.17 / 5.2	<u>0.17 / 5.0</u>	-/-	-/-	0.60 / 22.2	0.38 / 14.4
mount-norm	0.35 / 2.6	4.05 / 30.0	<b>0.08 / 0.7</b>	0.59 / 4.4	4.32 / 32.0	-/-	-/-	<u>0.09 / 0.8</u>	<u>0.09 / 0.8</u>
mount-fast	2.11 / 5.2	-/-	<b>0.11 / 3.7</b>	0.16 / 3.9	<u>0.13 / 3.1</u>	-/-	-/-	0.31 / 11.5	0.37 / 14.0
hdr-normal	0.64 / 1.9	1.27 / 3.8	<b>0.13 / 0.5</b>	0.57 / <u>1.7</u>	4.02 / 12.0	-/-	-/-	<u>0.52 / 2.4</u>	0.60 / 3.1
hdr-fast	0.22 / 4.0	0.30 / 5.5	<b>0.06 / 1.2</b>	0.21 / 3.9	<u>0.20 / 3.6</u>	-/-	-/-	0.20 / 4.6	0.24 / 5.7
corr-dolly	1.03 / 80	1.88 / 146	<u>0.56 / 54</u>	1.13 / 88	1.58 / 123	-/-	-/-	-/-	<b>0.51 / 53</b>
corr-walk	1.32 / 103	<u>0.50 / 39</u>	<u>0.54 / 50</u>	<b>0.43 / 34</b>	0.92 / 72	-/-	-/-	-/-	1.04 / 113
school-dolly	0.73 / 92	1.42 / 179	<b>0.11 / 16</b>	0.42 / 53	2.47 / 311	10.9 / 1371	-/-	4.61 / 651	<u>0.29 / 41</u>
school-scooter	0.70 / 75	<u>0.52 / 56</u>	<b>0.40 / 47</b>	0.59 / 63	1.30 / 139	9.21 / 983	-/-	0.55 / 66	<u>0.48 / 58</u>
units-dolly	7.64 / 1806	4.39 / 1039	<u>1.52 / 452</u>	3.43 / 812	5.84 / 1382	-/-	-/-	-/-	<b>0.48 / 131</b>
units-scooter	6.22 / 1450	4.92 / 1147	<u>1.67 / 497</u>	2.85 / 664	5.00 / 1166	-/-	-/-	3.69 / 1141	<b>0.88 / 296</b>

Table 2. VECtor dataset [16] with MPE[%/m] and ATE[cm]. Baseline numbers (except for DPVO and DPVO<sup>†</sup>) are taken from [7]. The first eleven sequences are small-scale, while the last six sequences cover large-scale scenes. Since events of the large-scale sequences are sparsely distributed, these sequences benefit strongly from our patch selection mechanism (*cf.* Sec. 4.2). Please note that methods utilizing frames have a considerable advantage due to the high-quality, global shutter FLIR Grasshopper3 camera with 1224 × 1024 pixels, while the event camera is a Prophesee Gen3 with 640 × 480 pixels from 2017. Moreover, the event stream exhibits significant artifacts due to the mounted infrared filter.

Method Modality	ORB3 [6]	VINS Fusion [40]	DPVO [53]	ESVIO [7]	PLEVIO [21]	DPVO <sup>†</sup>	DEVO (ours)
	Stereo VIO	Stereo VIO	Mono VO	Stereo EVIO	Mono EVIO	Mono EO <sup>†</sup>	Mono EO
	MPE / ATE	MPE / ATE	MPE / ATE	MPE / ATE	MPE / ATE	MPE / ATE	MPE / ATE
agg_tran	0.15 / 9.5	0.11 / 6.9	0.07 / 9.66	0.10 / 6.3	<u>0.07 / 4.8</u>	0.12 / 15.42	<b>0.06 / 4.03</b>
agg_rot	0.35 / 23.0	1.34 / 8.8	<b>0.04 / 3.70</b>	0.17 / 11.0	0.23 / 15.0	0.28 / 22.02	<u>0.05 / 3.58</u>
agg_flip*	<b>0.36 / 14.0</b>	1.16 / 45.0	0.99 / 56.52	<b>0.36 / 14.0</b>	<u>0.39 / 15.0</u>	1.16 / 60.26	0.71 / 44.90
agg_walk	-/-	-/-	1.17 / 107.4	<b>0.31 / 27.0</b>	<u>0.42 / 37.0</u>	-/-	0.90 / 88.27 <sup>‡</sup>
hdr_circle*	0.17 / 8.3	5.03 / 252.0	0.31 / 24.10	<u>0.16 / 8.1</u>	<b>0.14 / 6.8</b>	1.19 / 67.60	0.39 / 21.30
hdr_slow*	0.16 / 8.6	0.13 / 7.3	0.23 / 16.63	<u>0.11 / 5.9</u>	0.13 / 6.9	0.36 / 24.01	<b>0.08 / 4.95</b>
hdr_tran_rota	0.30 / 20.0	0.11 / 7.5	0.67 / 53.30	<u>0.10 / 6.5</u>	<u>0.10 / 6.8</u>	0.21 / 21.60	<b>0.08 / 5.91</b>
hdr_agg	0.29 / 28.0	1.21 / 118.0	0.29 / 36.10	<b>0.10 / 10.0</b>	<u>0.14 / 14.0</u>	0.54 / 59.80	0.26 / 33.98
hdr_dark_norm	-/-	0.86 / 80.0	-/-	<u>0.42 / 39.0</u>	1.35 / 125.0	0.49 / 47.70	<b>0.06 / 6.19</b>

Table 3. HKU dataset [7] with MPE[%/m] and ATE[cm]. Baseline numbers (except for DPVO and DPVO<sup>†</sup>) are taken from [7]. Note that the event-only VO methods EVO [42] and ESVO [69] fail on all sequences of the HKU dataset (*cf.* [7]). Sequences marked with (\*) contain 2-6 subsequent voxel grids with sensor detection failures on at least 80% of the sensor array, making tracking hard at fast motion without additional modality. Results marked with (‡) use top-*P* sampling, otherwise DEVO fails with multinomial sampling.

sequences. DEVO is only beaten on *rpg\_bin* by DPVO (mono VO) and ORB-SLAM2 [38] (stereo VO).

**MVSEC** The MVSEC dataset [70] provides stereo events and frames from two DAVIS346. We compare to previous work [7] on the indoor flying room. In Tab. 7, we surpass all related work, except DPVO, by large margins on all sequences. The event-only methods EVO and ESVO fail on at least one sequence. We attain an average ATE of 65% lower than ESVIO, which utilizes stereo events, stereo frames, and IMU. DEVO performs worse than frame-based DPVO, which might be due to the noisy event data of MVSEC. The event stream of MVSEC exhibits a negative-to-positive polarity ratio of 3.2, which is by far the largest among all seven real-world datasets: EDS (1.5), FPV (1.5), VECtor (1.2), HKU (0.8), RPG (0.7), TUM-VIE (0.7). This noisy event

stream also leads to artifacts in the E2VID reconstructions, resulting in failures of DPVO<sup>†</sup> on all sequences.

## 4.2. Ablation Study

We perform ablation experiments on seven real-world event VO benchmarks to study our contributions. We run each sequence five times, take the median per sequence, and report the average of medians per dataset.

**Photometric voxel augmentation** In Tab. 8, DEVO benefits from photometric augmentation on all datasets, except on VECtor [16], where it shows a less than 3.6% accuracy drop. Voxel grids of the training dataset follow an ideal event generation model (*cf.* Eq. (1)). One prominent effect of our photometric augmentation is to reduce event density. Particularly, the UZH-FPV [8] dataset benefits strongly.

Method Modality	ORB-SLAM3 [6]			DPVO [53]			DPVO <sup>†</sup>			DEVO (ours)		
	Mono VO			Mono VO			Mono EO <sup>†</sup>			Mono EO		
	ATE	R <sub>rmse</sub>	MPE	ATE	R <sub>rmse</sub>	MPE	ATE	R <sub>rmse</sub>	MPE	ATE	R <sub>rmse</sub>	MPE
peanuts_dark	6.15	11.40	0.49	<b>1.26</b>	<b>1.83</b>	<b>0.12</b>	5.76	8.55	0.52	4.78	2.49	0.30
peanuts_light	27.26	6.88	1.14	<b>12.99</b>	<b>2.66</b>	<b>0.44</b>	69.77	13.83	2.36	<u>21.07</u>	<u>3.84</u>	<u>0.75</u>
peanuts_run	<b>16.83</b>	<b>5.78</b>	<b>0.19</b>	<u>25.48</u>	<u>11.19</u>	<u>0.29</u>	43.49	19.72	0.52	38.10	18.28	0.43
rocket_dark	<u>10.12</u>	9.75	<u>0.37</u>	27.41	<u>5.23</u>	1.07	80.89	24.43	3.65	<b>8.78</b>	<b>4.16</b>	<b>0.32</b>
rocket_light	<b>32.53</b>	11.39	<b>1.79</b>	63.11	<u>10.44</u>	3.64	97.62	24.86	5.08	<u>59.83</u>	<b>9.28</b>	<u>3.40</u>
ziggy	26.92	4.42	0.42	14.86	<u>3.45</u>	<u>0.22</u>	23.79	6.29	0.36	<b>11.84</b>	<b>2.32</b>	<b>0.15</b>
ziggy_hdr	81.98	17.67	1.13	66.17	<u>10.32</u>	1.02	<u>46.41</u>	15.84	<u>0.72</u>	<b>22.82</b>	<b>9.07</b>	<b>0.36</b>
ziggy_flying	20.57	8.02	1.33	<b>10.85</b>	3.66	<u>0.73</u>	34.51	9.04	2.05	<u>10.92</u>	<b>3.39</b>	<b>0.71</b>
all_chars	<u>21.37</u>	<u>9.02</u>	<u>0.27</u>	95.87	29.00	1.39	76.02	14.86	0.90	<b>10.76</b>	<b>3.62</b>	<b>0.16</b>

Table 4. EDS dataset [24] with ATE[cm], R<sub>rmse</sub>[deg], and mean position error MPE[%/m]. Since events of the EDS dataset are more densely populated than in the other datasets, we reduce the time window for each event voxel grid by half. Our method performs clearly better than DPVO on *rocket\_dark*, *ziggy\_hdr*, and *all\_chars* due to HDR and very fast motion.

Method	Modality	1d-trans	3d-trans	6dof	desk	desk2
ORB-SLAM3 [6]	Stereo VIO	0.7	1.2	1.8	<b>0.7</b>	2.5
BASALT [55]	Stereo VIO	<b>0.3</b>	<u>0.9</u>	<u>1.4</u>	1.6	1.1
DPVO [53]	Mono VO	<u>0.5</u>	1.1	<b>1.2</b>	<u>1.2</u>	<b>0.8</b>
DH-PTAM [47]	Stereo EVO	10.3	<b>0.7</b>	2.4	1.6	1.5
USLAM [56]	Mono EVIO	3.9	4.7	35.3	19.5	34.1
ESVO [69]	Stereo EO	0.9	2.8	5.8	3.3	3.2
EVO [42]	Mono EO	7.5	12.5	85.5	54.1	75.2
DPVO <sup>†</sup>	Mono EO <sup>†</sup>	2.3	8.2	7.9	5.1	3.7
<b>DEVO (ours)</b>	Mono EO	<u>0.5</u>	1.1	1.6	1.7	<u>1.0</u>

Table 5. TUM-VIE dataset [29] with ATE[cm] on the ‘‘mocap’’ sequences. Baseline numbers (except for DPVO and DPVO<sup>†</sup>) are taken from [47]. DEVO beats the event-only methods (DPVO<sup>†</sup>, EVO, and ESVO) by large margins on all sequences (at least 44% lower ATE).

Dataset	w/o photo. Aug.		with photo. Aug.	
	ATE	#fails	ATE	#fails
UZH-FPV [8]	132.18	1	<b>107.01</b>	2
VECTor [16]	<b>42.52</b>	0	44.03	0
HKU [7]	17.26	7	<b>15.60</b>	6
EDS [24]	23.24	4	<b>20.99</b>	4
TUM-VIE [29]	1.38	0	<b>1.20</b>	0
RPG [68]	1.00	0	<b>0.97</b>	0
MVSEC [70]	13.37	1	<b>11.08</b>	0
All datasets	32.99	13	<b>28.70</b>	<b>12</b>

Table 8. Ablation study of photometric voxel augmentation. Average ATE[cm] and total number of failures (#fails) for seven real-world datasets. Our proposed photometric augmentation improves accuracy and robustness.

**Patch selection and sampling** Table 9 shows that our learned score map improves the pose tracking accuracy over random or gradient-based sampling during training and inference. It also shows that our grid-based pooled multinomial sampling on the learned score map achieves the best results for the majority of the datasets with the smallest number of failures. Our multinomial sampling without grid ranks second on average ATE, but it is less robust, especially on MVSEC. While the gradient-based method

performs slightly better on RPG and TUM-VIE, our proposed method shows the best accuracy on more challenging scenes. Top- $P$  sampling performs significantly worse than our method. Employing the grid improves robustness (12 failures w/ grid vs. 16 failures w/o), which is expected for sparse event data. The proposed average pooling before sampling increases accuracy and robustness on average.

## 5. Conclusion

We present DEVO, a monocular event-only VO with strong performance on seven real-world benchmarks. Our method tracks sparse event patches over time, extracted by our learned patch selector and pooled multinomial sampling mechanism. Our results clearly show the benefit of using event cameras for VO in challenging scenarios. We show that learning-based VO for events is a promising direction. Our work is the first to train on a huge, simulated training dataset of events showing strong generalization to the real world. Future work could investigate using even larger, more diverse datasets for training or more realistic noise models for event simulation. Another interesting direction is to combine DEVO with other sensors.

**Acknowledgments** This work was supported by the ERC Advanced Grant SIMULACRON.

Method	Modality	rpg_bin		rpg_boxes2		rpg_desk2		rpg_monitor2	
		ATE	$R_{\text{rmse}}$	ATE	$R_{\text{rmse}}$	ATE	$R_{\text{rmse}}$	ATE	$R_{\text{rmse}}$
ORB-SLAM2 [38]	Stereo VO	<b>0.7</b>	<u>0.58</u>	<u>1.6</u>	4.26	1.8	2.81	<u>0.8</u>	3.70
ORB-SLAM2 [38]	Mono VO	2.4	0.84	3.9	2.39	3.8	2.52	3.1	1.77
DSO [12]	Mono VO	1.1	2.12	2.0	2.14	10.0	63.5	0.9	<b>0.33</b>
DPVO [53]	Mono VO	<b>0.7</b>	<b>0.4</b>	1.62	<u>1.78</u>	3.1	<u>1.04</u>	2.12	2.08
USLAM [56]	Mono EVIO	7.7	7.18	9.5	8.84	9.8	32.46	6.5	7.01
EDSO [24]	Mono EVO	1.1	0.99	2.1	1.83	<u>1.5</u>	1.87	1.0	<u>0.60</u>
ESVO [69]	Stereo EO	2.8	7.61	5.8	9.46	3.2	7.25	3.3	2.74
EVO [42]	Mono EO	13.2*	50.26*	14.2*	170.36*	5.2	8.25	7.8	7.77
DPVO <sup>†</sup>	Mono EO <sup>†</sup>	4.00	3.23	4.20	2.87	3.05	1.45	2.35	2.79
<b>DEVO (ours)</b>	Mono EO	<u>1.03</u>	0.86	<b>0.92</b>	<b>0.70</b>	<b>1.21</b>	<b>0.95</b>	<b>0.71</b>	1.04

Table 6. RPG dataset [68] with ATE[cm] and  $R_{\text{rmse}}$ [deg]. Baseline numbers (except for DPVO and DPVO<sup>†</sup>) are taken from [25]. Results marked with (\*) indicate failure after completing at most 30% of the sequence. DEVO outperforms the event-only methods (DPVO<sup>†</sup>, EVO, and ESVO) by large margins on all sequences (at least 63% lower ATE). In addition, we attain an average ATE 88% lower than USLAM (mono EVIO) and 28% lower than EDSO (mono EVO).

Method	Modality	Indoor Fly1	Indoor Fly2	Indoor Fly3	Indoor Fly4
		MPE / ATE	MPE / ATE	MPE / ATE	MPE / ATE
ORB-SLAM3 [6]	Stereo VIO	5.31 / 142.0	5.65 / 170.0	2.90 / 154.0	6.99 / 58.0
VINS Fusion [40]	Stereo VIO	1.50 / 40.0	6.98 / 210.0	0.73 / 39.0	3.62 / 30.0
DPVO [53]	Mono VO	<b>0.16 / 4.8</b>	<b>0.15 / 6.3</b>	<b>0.08 / 4.6</b>	<b>0.30 / 3.2</b>
ESVIO [7]	Stereo EVIO	0.94 / 25.0	1.00 / 30.0	0.47 / 25.0	5.55 / 46.0
USLAM [56]	Mono EVIO	- / -	- / -	- / -	2.77 / 23.0
PLEVIO [21]	Mono EVIO	1.35 / 36.0	1.00 / 30.0	0.64 / 34.0	5.31 / 44.0
ESVO [69]	Stereo EO	4.00 / 107.0	3.66 / 110.0	1.71 / 91.0	- / -
EVO [42]	Mono EO	5.09 / 136.0	- / -	2.58 / 137.0	- / -
DPVO <sup>†</sup>	Mono EO <sup>†</sup>	- / -	- / -	- / -	- / -
<b>DEVO (ours)</b>	Mono EO	<u>0.26 / 7.76</u>	<u>0.32 / 13.30</u>	<u>0.19 / 10.72</u>	<u>1.08 / 12.57</u>

Table 7. MVSEC dataset [70] with MPE[%/m] and ATE[cm]. Baseline numbers (except for DPVO and DPVO<sup>†</sup>) are taken from [7]. DEVO is the first event-only method that does not fail on any sequence of MVSEC. DEVO performs substantially better than all prior work, except DPVO, on all sequences. DEVO performs worse than DPVO, which might be due to the biased polarity ratio of the event data.

Training	random	gradient	score map (ours)				
	random	pool-grid	3P-random	top-P samp.	multinomial sampling		
Settings				pool-grid	w/o pool.	w/o grid	pool-grid
	ATE / #	ATE / #	ATE / #	ATE / #	ATE / #	ATE / #	ATE / #
UZH-FPV [8]	190.11 / 2	128.93 / 0	121.19 / 4	111.85 / 0	142.63 / 3	<u>109.33</u> / 2	<b>107.01</b> / 2
VECTOR [16]	70.16 / 0	106.27 / 0	63.97 / 0	68.01 / 0	64.40 / 0	<u>52.92</u> / 0	<b>44.03</b> / 0
HKU [7]	21.56 / 10	<u>15.67</u> / 8	18.62 / 8	18.99 / 2	20.87 / 7	18.18 / 5	<b>15.60</b> / 6
EDS [24]	<u>24.08</u> / 4	31.64 / 5	27.95 / 3	33.63 / 8	36.44 / 7	28.13 / 4	<b>20.99</b> / 4
TUM-VIE [29]	1.49 / 0	<b>1.16</b> / 0	1.18 / 0	1.25 / 0	1.18 / 0	<u>1.17</u> / 0	1.20 / 0
RPG [68]	1.02 / 0	<b>0.92</b> / 0	1.14 / 0	1.04 / 0	1.18 / 0	1.11 / 0	<u>0.97</u> / 0
MVSEC [70]	<b>11.02</b> / 0	13.01 / 2	27.10 / 2	13.11 / 4	13.61 / 1	34.16 / 5	<u>11.08</u> / 0
All datasets	45.63 / 16	42.51 / 15	37.31 / 17	35.41 / <u>14</u>	40.04 / 18	<u>35.00</u> / 16	<b>28.70</b> / 12

Table 9. Ablation study on patch selection methods during training and respective patch sampling at inference evaluated on seven real-world datasets. Average ATE[cm] and total number of failures (#) for each dataset. DPVO [53] employs random patch selection during training and inference for dense RGB data, which does not work well for events. Our proposed grid-based pooled multinomial sampling on the learned score map performs best on four of seven datasets with the smallest number of failures. Pool refers to  $4 \times 4$  average pooling before sampling. Refer to Sec. 3.2 for a detailed description of all sampling methods.



## References

- [1] Christian Brandli, Raphael Berner, Minhao Yang, Shih-Chii Liu, and Tobi Delbruck. A  $240 \times 180$  130 db 3  $\mu$ s latency global shutter spatiotemporal vision sensor. *IEEE Journal of Solid-State Circuits*, 49(10):2333–2341, 2014. 2, 5
- [2] Samuel Bryner, Guillermo Gallego, Henri Rebecq, and Davide Scaramuzza. Event-based, direct camera tracking from a photometric 3d map using nonlinear optimization. In *2019 International Conference on Robotics and Automation (ICRA)*, pages 325–331. IEEE, 2019. 2
- [3] Russell Buchanan, Varun Agrawal, Marco Camurri, Frank Dellaert, and Maurice Fallon. Deep imu bias inference for robust visual-inertial odometry with factor graphs. *IEEE Robotics and Automation Letters*, 8(1):41–48, 2022. 2
- [4] Cesar Cadena, Luca Carlone, Henry Carrillo, Yasir Latif, Davide Scaramuzza, José Neira, Ian Reid, and John J Leonard. Past, present, and future of simultaneous localization and mapping: Toward the robust-perception age. *IEEE Transactions on robotics*, 32(6):1309–1332, 2016. 1
- [5] Zhiao Cai, Ming Yang, Chunxiang Wang, and Bing Wang. Monocular visual-inertial odometry based on sparse feature selection with adaptive grid. In *2018 IEEE Intelligent Vehicles Symposium (IV)*, pages 1842–1847. IEEE, 2018. 4
- [6] Carlos Campos, Richard Elvira, Juan J Gómez Rodríguez, José MM Montiel, and Juan D Tardós. Orb-slam3: An accurate open-source library for visual, visual-inertial, and multi-map slam. *IEEE Transactions on Robotics*, 37(6):1874–1890, 2021. 5, 6, 7, 8
- [7] Peiyu Chen, Weipeng Guan, and Peng Lu. Esvio: Event-based stereo visual inertial odometry. *IEEE Robotics and Automation Letters*, 2023. 1, 2, 5, 6, 7, 8
- [8] Jeffrey Delmerico, Titus Cieslewski, Henri Rebecq, Matthias Faessler, and Davide Scaramuzza. Are we ready for autonomous drone racing? the uzh-fpv drone racing dataset. In *2019 International Conference on Robotics and Automation (ICRA)*, pages 6713–6719. IEEE, 2019. 4, 5, 6, 7, 8
- [9] Daniel DeTone, Tomasz Malisiewicz, and Andrew Rabinovich. Self-improving visual odometry. *arXiv preprint arXiv:1812.03245*, 2018. 2
- [10] Alexey Dosovitskiy, German Ros, Felipe Codevilla, Antonio Lopez, and Vladlen Koltun. CARLA: An open urban driving simulator. In *Proceedings of the 1st Annual Conference on Robot Learning*, pages 1–16, 2017. 2
- [11] Jakob Engel, Thomas Schöps, and Daniel Cremers. Lsdslam: Large-scale direct monocular slam. In *European conference on computer vision*, pages 834–849. Springer, 2014. 3
- [12] Jakob Engel, Vladlen Koltun, and Daniel Cremers. Direct sparse odometry. *IEEE transactions on pattern analysis and machine intelligence*, 40(3):611–625, 2017. 2, 3, 8
- [13] Christian Forster, Matia Pizzoli, and Davide Scaramuzza. Svo: Fast semi-direct monocular visual odometry. In *2014 IEEE international conference on robotics and automation (ICRA)*, pages 15–22. IEEE, 2014. 2
- [14] Guillermo Gallego, Christian Forster, Elias Mueggler, and Davide Scaramuzza. Event-based camera pose tracking using a generative event model. *arXiv preprint arXiv:1510.01972*, 2015. 2
- [15] Guillermo Gallego, Tobi Delbrück, Garrick Orchard, Chiara Bartolozzi, Brian Taba, Andrea Censi, Stefan Leutenegger, Andrew J. Davison, Jörg Conradt, Kostas Daniilidis, and Davide Scaramuzza. Event-based vision: A survey. *IEEE TPAMI*, 44(1):154–180, 2022. 1, 3
- [16] Ling Gao, Yuxuan Liang, Jiaqi Yang, Shaoxun Wu, Chenyu Wang, Jiaben Chen, and Laurent Kneip. Vector: A versatile event-centric benchmark for multi-sensor slam. *IEEE Robotics and Automation Letters*, 7(3):8217–8224, 2022. 5, 6, 7, 8
- [17] Xiang Gao, Rui Wang, Nikolaus Demmel, and Daniel Cremers. Ldso: Direct sparse odometry with loop closure. In *2018 IEEE/RSJ International Conference on Intelligent Robots and Systems (IROS)*, pages 2198–2204. IEEE, 2018. 3
- [18] Aykut G Gelen and Ayten Atasoy. An artificial neural slam framework for event-based vision. *IEEE Access*, 2023. 2
- [19] Michael Grupp. evo: Python package for the evaluation of odometry and slam. <https://github.com/MichaelGrupp/evo>, 2017. 5
- [20] Weipeng Guan and Peng Lu. Monocular event visual inertial odometry based on event-corner using sliding windows graph-based optimization. In *2022 IEEE/RSJ International Conference on Intelligent Robots and Systems (IROS)*, pages 2438–2445. IEEE, 2022. 2
- [21] Weipeng Guan, Peiyu Chen, Yuhang Xie, and Peng Lu. Pl-evio: Robust monocular event-based visual inertial odometry with point and line features. *arXiv preprint arXiv:2209.12160*, 2022. 1, 2, 5, 6, 8
- [22] Xiao Han, Yulin Tao, Zhuyi Li, Ruping Cen, and Fangzheng Xue. Superpointvo: A lightweight visual odometry based on cnn feature extraction. In *2020 5th International Conference on Automation, Control and Robotics Engineering (CACRE)*, pages 685–691. IEEE, 2020. 2
- [23] Chris Harris, Mike Stephens, et al. A combined corner and edge detector. In *Alvey vision conference*, pages 10–5244. Citeseer, 1988. 2
- [24] Javier Hidalgo-Carrió, Guillermo Gallego, and Davide Scaramuzza. Event-aided direct sparse odometry. In *CVPR*, 2022. 1, 2, 4, 5, 7, 8
- [25] Kunping Huang, Sen Zhang, Jing Zhang, and Dacheng Tao. Event-based simultaneous localization and mapping: A comprehensive survey. *arXiv preprint arXiv:2304.09793*, 2023. 8
- [26] Iman Abaspor Kazerouni, Luke Fitzgerald, Gerard Dooly, and Daniel Toal. A survey of state-of-the-art on visual slam. *Expert Systems with Applications*, 205:117734, 2022. 2
- [27] Haram Kim and H Jin Kim. Real-time rotational motion estimation with contrast maximization over globally aligned events. *IEEE Robotics and Automation Letters*, 6(3):6016–6023, 2021. 2
- [28] Hanme Kim, Stefan Leutenegger, and Andrew J Davison. Real-time 3d reconstruction and 6-dof tracking with an event camera. In *Computer Vision—ECCV 2016: 14th European Conference, Amsterdam, The Netherlands, October 11–14,*

- 2016, *Proceedings, Part VI 14*, pages 349–364. Springer, 2016. [2](#)
- [29] Simon Klenk, Jason Chui, Nikolaus Demmel, and Daniel Cremers. Tum-vie: The tum stereo visual-inertial event dataset. In *2021 IEEE/RSJ International Conference on Intelligent Robots and Systems (IROS)*, pages 8601–8608. IEEE, 2021. [5](#), [7](#), [8](#)
- [30] Beat Kueng, Elias Mueggler, Guillermo Gallego, and Davide Scaramuzza. Low-latency visual odometry using event-based feature tracks. In *2016 IEEE/RSJ International Conference on Intelligent Robots and Systems (IROS)*, pages 16–23, 2016. [2](#)
- [31] Cedric Le Gentil, Florian Tschopp, Ignacio Alzugaray, Teresa Vidal-Calleja, Roland Siegwart, and Juan Nieto. Idol: A framework for imu-dvs odometry using lines. In *2020 IEEE/RSJ International Conference on Intelligent Robots and Systems (IROS)*, pages 5863–5870. IEEE, 2020. [2](#)
- [32] Philipp Lindenberger, Paul-Edouard Sarlin, Viktor Larsson, and Marc Pollefeys. Pixel-perfect structure-from-motion with featuremetric refinement. In *Proceedings of the IEEE/CVF international conference on computer vision*, pages 5987–5997, 2021. [3](#)
- [33] Daqi Liu, Alvaro Parra, and Tat-Jun Chin. Globally optimal contrast maximisation for event-based motion estimation. In *Proceedings of the IEEE/CVF Conference on Computer Vision and Pattern Recognition*, pages 6349–6358, 2020. [2](#)
- [34] Daqi Liu, Alvaro Parra, and Tat-Jun Chin. Spatiotemporal registration for event-based visual odometry. In *Proceedings of the IEEE/CVF Conference on Computer Vision and Pattern Recognition*, pages 4937–4946, 2021. [2](#)
- [35] Guoyu Lu, Liqiang Nie, Scott Sorensen, and Chandra Kambhampettu. Large-scale tracking for images with few textures. *IEEE Transactions on Multimedia*, 19(9):2117–2128, 2017. [4](#)
- [36] Florian Mahlknecht, Daniel Gehrig, Jeremy Nash, Friedrich M Rockenbauer, Benjamin Morrell, Jeff DeLaune, and Davide Scaramuzza. Exploring event camera-based odometry for planetary robots. *IEEE Robotics and Automation Letters*, 7(4):8651–8658, 2022. [2](#)
- [37] Elias Mueggler, Guillermo Gallego, Henri Rebecq, and Davide Scaramuzza. Continuous-time visual-inertial odometry for event cameras. *IEEE Transactions on Robotics*, 34(6):1425–1440, 2018. [2](#)
- [38] Raul Mur-Artal and Juan D Tardós. Orb-slam2: An open-source slam system for monocular, stereo, and rgb-d cameras. *IEEE transactions on robotics*, 33(5):1255–1262, 2017. [2](#), [6](#), [8](#)
- [39] Tong Qin, Peiliang Li, and Shaojie Shen. Vins-mono: A robust and versatile monocular visual-inertial state estimator. *IEEE Transactions on Robotics*, 34(4):1004–1020, 2018. [5](#)
- [40] Tong Qin, Jie Pan, Shaozu Cao, and Shaojie Shen. A general optimization-based framework for local odometry estimation with multiple sensors. *arXiv preprint arXiv:1901.03638*, 2019. [5](#), [6](#), [8](#)
- [41] Henri Rebecq, Guillermo Gallego, and Davide Scaramuzza. Emvs: Event-based multi-view stereo. 2016. [2](#)
- [42] Henri Rebecq, Timo Horstschäfer, Guillermo Gallego, and Davide Scaramuzza. Evo: A geometric approach to event-based 6-dof parallel tracking and mapping in real time. *IEEE Robotics and Automation Letters*, 2(2):593–600, 2016. [1](#), [2](#), [5](#), [6](#), [7](#), [8](#)
- [43] Henri Rebecq, Timo Horstschaefer, and Davide Scaramuzza. Real-time visual-inertial odometry for event cameras using keyframe-based nonlinear optimization. 2017. [2](#)
- [44] Henri Rebecq, Daniel Gehrig, and Davide Scaramuzza. Esim: an open event camera simulator. In *Conference on robot learning*, pages 969–982. PMLR, 2018. [3](#), [4](#)
- [45] Henri Rebecq, René Ranftl, Vladlen Koltun, and Davide Scaramuzza. Events-to-video: Bringing modern computer vision to event cameras. In *CVPR*, pages 3857–3866, 2019. [4](#)
- [46] Christian Reinbacher, Gottfried Munda, and Thomas Pock. Real-time panoramic tracking for event cameras. In *2017 IEEE International Conference on Computational Photography (ICCP)*, pages 1–9. IEEE, 2017. [2](#)
- [47] Abanob Soliman, Fabien Bonardi, Désiré Sidibé, and Samia Bouchafa. Dh-ptam: A deep hybrid stereo events-frames parallel tracking and mapping system. *arXiv preprint arXiv:2306.01891*, 2023. [5](#), [7](#)
- [48] Timo Stoffregen, Cedric Scheerlinck, Davide Scaramuzza, Tom Drummond, Nick Barnes, Lindsay Kleeman, and Robert Mahony. Reducing the sim-to-real gap for event cameras. In *Computer Vision—ECCV 2020: 16th European Conference, Glasgow, UK, August 23–28, 2020, Proceedings, Part XXVII 16*, pages 534–549. Springer, 2020. [2](#)
- [49] Jürgen Sturm, Nikolas Engelhard, Felix Endres, Wolfram Burgard, and Daniel Cremers. A benchmark for the evaluation of rgb-d slam systems. In *2012 IEEE/RSJ international conference on intelligent robots and systems*, pages 573–580. IEEE, 2012. [5](#)
- [50] Chengzhou Tang and Ping Tan. Ba-net: Dense bundle adjustment network. *arXiv preprint arXiv:1806.04807*, 2018. [3](#)
- [51] Zachary Teed and Jia Deng. Raft: Recurrent all-pairs field transforms for optical flow. In *Computer Vision—ECCV 2020: 16th European Conference, Glasgow, UK, August 23–28, 2020, Proceedings, Part II 16*, pages 402–419. Springer, 2020. [2](#)
- [52] Zachary Teed and Jia Deng. Droid-slam: Deep visual slam for monocular, stereo, and rgb-d cameras. *Advances in neural information processing systems*, 34:16558–16569, 2021. [1](#), [2](#)
- [53] Zachary Teed, Lahav Lipson, and Jia Deng. Deep patch visual odometry. *arXiv preprint arXiv:2208.04726*, 2022. [1](#), [2](#), [3](#), [4](#), [5](#), [6](#), [7](#), [8](#)
- [54] Benjamin Ummenhofer, Huizhong Zhou, Jonas Uhrig, Nikolaus Mayer, Eddy Ilg, Alexey Dosovitskiy, and Thomas Brox. Demon: Depth and motion network for learning monocular stereo. In *Proceedings of the IEEE conference on computer vision and pattern recognition*, pages 5038–5047, 2017. [2](#)
- [55] Vladislav Usenko, Nikolaus Demmel, David Schubert, Jörg Stückler, and Daniel Cremers. Visual-inertial mapping with

- non-linear factor recovery. *IEEE Robotics and Automation Letters*, 5(2):422–429, 2019. 1, 2, 4, 7
- [56] Antoni Rosinol Vidal, Henri Rebecq, Timo Horstschaefer, and Davide Scaramuzza. Ultimate slam? combining events, images, and imu for robust visual slam in hdr and high-speed scenarios. *IEEE RA-L*, 2018. 1, 2, 5, 7, 8
- [57] Lukas Von Stumberg and Daniel Cremers. Dm-vio: Delayed marginalization visual-inertial odometry. *IEEE Robotics and Automation Letters*, 7(2):1408–1415, 2022. 2
- [58] Sen Wang, Ronald Clark, Hongkai Wen, and Niki Trigoni. Deepvo: Towards end-to-end visual odometry with deep recurrent convolutional neural networks. In *2017 IEEE international conference on robotics and automation (ICRA)*, pages 2043–2050. IEEE, 2017. 2
- [59] Wenshan Wang, DeLong Zhu, Xiangwei Wang, Yaoyu Hu, Yuheng Qiu, Chen Wang, Yafei Hu, Ashish Kapoor, and Sebastian Scherer. Tartanair: A dataset to push the limits of visual slam. 2020. 4
- [60] Wenshan Wang, Yaoyu Hu, and Sebastian Scherer. Tartanvo: A generalizable learning-based vo. In *Conference on Robot Learning*, pages 1761–1772. PMLR, 2021. 1, 2
- [61] Yifu Wang, Jiaqi Yang, Xin Peng, Peng Wu, Ling Gao, Kun Huang, Jiaben Chen, and Laurent Kneip. Visual odometry with an event camera using continuous ray warping and volumetric contrast maximization. *Sensors*, 22(15):5687, 2022. 2
- [62] David Weikersdorfer, David B Adrian, Daniel Cremers, and Jörg Conradt. Event-based 3d slam with a depth-augmented dynamic vision sensor. In *2014 IEEE international conference on robotics and automation (ICRA)*, pages 359–364. IEEE, 2014. 2
- [63] Chengxi Ye, Anton Mitrokhin, Cornelia Fermüller, James A Yorke, and Yiannis Aloimonos. Unsupervised learning of dense optical flow, depth and egomotion from sparse event data. *arXiv preprint arXiv:1809.08625*, 2018. 2
- [64] Wenzhen Yuan and Srikumar Ramalingam. Fast localization and tracking using event sensors. In *2016 IEEE International Conference on Robotics and Automation (ICRA)*, pages 4564–4571. IEEE, 2016. 2
- [65] Huangying Zhan, Chamara Saroj Weerasekera, Jia-Wang Bian, and Ian Reid. Visual odometry revisited: What should be learnt? In *2020 IEEE international conference on robotics and automation (ICRA)*, pages 4203–4210. IEEE, 2020. 1, 2
- [66] Zichao Zhang and Davide Scaramuzza. A tutorial on quantitative trajectory evaluation for visual (-inertial) odometry. In *2018 IEEE/RSJ International Conference on Intelligent Robots and Systems (IROS)*, pages 7244–7251. IEEE, 2018. 5
- [67] Huizhong Zhou, Benjamin Ummenhofer, and Thomas Brox. Deeptam: Deep tracking and mapping. In *Proceedings of the European conference on computer vision (ECCV)*, pages 822–838, 2018. 2
- [68] Yi Zhou, Guillermo Gallego, Henri Rebecq, Laurent Kneip, Hongdong Li, and Davide Scaramuzza. Semi-dense 3d reconstruction with a stereo event camera. In *Proceedings of the European conference on computer vision (ECCV)*, pages 235–251, 2018. 4, 5, 7, 8
- [69] Yi Zhou, Guillermo Gallego, and Shaojie Shen. Event-based stereo visual odometry. *IEEE Transactions on Robotics*, 37(5):1433–1450, 2021. 5, 6, 7, 8
- [70] Alex Zihao Zhu, Dinesh Thakur, Tolga Özaslan, Bernd Pfrommer, Vijay Kumar, and Kostas Daniilidis. The multi-vehicle stereo event camera dataset: An event camera dataset for 3d perception. *IEEE Robotics and Automation Letters*, 3(3):2032–2039, 2018. 2, 4, 6, 7, 8
- [71] Alex Zihao Zhu, Liangzhe Yuan, Kenneth Chaney, and Kostas Daniilidis. Unsupervised event-based learning of optical flow, depth, and egomotion. In *Proceedings of the IEEE/CVF Conference on Computer Vision and Pattern Recognition*, pages 989–997, 2019. 2
- [72] Dekai Zhu, Zhongcong Xu, Jinhu Dong, Canbo Ye, Yinbai Hu, Hang Su, Zhengfa Liu, and Guang Chen. Neuromorphic visual odometry system for intelligent vehicle application with bio-inspired vision sensor. In *2019 IEEE International Conference on Robotics and Biomimetics (ROBIO)*, pages 2225–2232. IEEE, 2019. 2
- [73] Alex Zihao Zhu, Nikolay Atanasov, and Kostas Daniilidis. Event-based visual inertial odometry. In *Proceedings of the IEEE Conference on Computer Vision and Pattern Recognition*, pages 5391–5399, 2017. 2
- [74] Yi-Fan Zuo, Jiaqi Yang, Jiaben Chen, Xia Wang, Yifu Wang, and Laurent Kneip. Devo: Depth-event camera visual odometry in challenging conditions. In *2022 International Conference on Robotics and Automation (ICRA)*, pages 2179–2185. IEEE, 2022. 2